OBSERVATIONAL STUDY OF SNOW CORNICE DEVELOPMENT ON ARTIFICIAL VERTICAL SECTIONS

TakahiroTanabe[1]*, Kouichi Nshimura[2], Taiki Nunokawa[2], Yoshihiko Saito[2], Tsubasa Okaze[3], Satoru Adachi[1], Satoru Yamaguchi[4], Yoichi Ito[4], Sojiro Sunako[4], and Hirofumi Niiya[5]

[1] National Research Institute for Earth Science and Disaster Resilience, Yamagata, Japan
2 Yukiken Snow Eaters, Hokkaido, Japan
3 Institute of Science Tokyo, Kanagawa, Japan
4 National Research Institute for Earth Science and Disaster Resilience, Niigata, Japan
5 Niigata University, Niigata, Japan

ABSTRACT: Snow cornices are overhanging accumulations of wind-transported snow that frequently develop along mountain ridges and may trigger avalanches when they collapse. Although previous studies have documented the seasonal evolution of cornices, the short-term processes governing their formation remain poorly understood because continuous field observations are scarce. In this study, we conducted a field observation campaign at Niseko Moiwa Ski Resort, Hokkaido, Japan, during a blowing-snow event from 7 to 8 March 2026. Artificial vertical snow sections were prepared prior to the event, and the temporal evolution of cornice growth was monitored using a 2D line LiDAR. Wind speed, wind direction, blowing-snow mass flux, snow surface elevation were also measured, together with UAV-mounted LiDAR surveys and visual observations. The observations revealed rapid cornice development around midnight, during which the cornice thickness increased by several centimeters within 10 min. The vertical profiles showed a repeating pattern consisting of two successive stagse: snow first accumulated several meters upwind of the vertical section, followed by deposition immediately adjacent to the section. Repetition of these stages resulted in progressive outward cornice growth. Simultaneously, snow accumulated beneath the overhang until it merged with the upper snowpack to form a continuous slope. In contrast, no distinctive changes in wind speed, gust factor, or blowing-snow mass flux were associated with the rapid growth period. These observations suggest that cornice growth results from the simultaneous development of the overhanging snow and the underlying snowpack, rather than solely from snow adhering to the underside of the overhang. The results provide new insights into the short-term snow cornice formation processes and offer valuable information for improving hazard assessment and winter mountain safety.

KEYWORDS: Snow cornice; blowing snow; ski resort; hazard assessment.

1. INTRODUCTION

Wind-driven snow transport produces a variety of snow surface patterns and bedforms (Kochanski et al., 2019). Among these features, an overhanging accumulation of wind-transported snow formed along a mountain ridge is referred to as a snow cornice. Snow cornices pose a significant hazard because their collapse can trigger avalanches or directly threaten people traveling in mountainous terrain (Vogel et al., 2012).

To improve our understanding of snow cornice dynamics, previous studies have employed field observations (Vogel et al., 2012; Hancock et al., 2020), wind-tunnel experiments (Yu et al., 2023, 2025a), and numerical simulations (Yu et al., 2025b). In particular, previous field observations have documented the seasonal evolution of snow cornices over periods of several months. However, the short-term processes governing rapid cornice formation remain poorly understood because continuous field observations at high temporal resolution remain scarce. Furthermore, because the internal structure of a natural cornice is difficult to observe directly, the processes by which an overhang develops and merges with the underlying snowpack remain unclear.

In this study, we present field observations of rapid snow cornice development during a single overnight blowing-snow event. Artificial vertical snow sections were prepared to facilitate direct observation of the evolving cornice geometry and internal snow structure. By continuously monitoring the vertical cross-sectional snow profile using a 2D line LiDAR, we captured the temporal evolution of the snowpack structure associated with rapid cornice growth. These observations provide new insights into the short-term processes of snow cornice formation.

* Corresponding author address:
Takahiro Tanabe, National Research Institute for Earth Science and Disaster Resilience,
Shinjo, Yamagata, Japan, 996-0091;
tel: +81 233-23-8003; fax: +81 233-22-7554
email: tnabe@bosai.go.jp

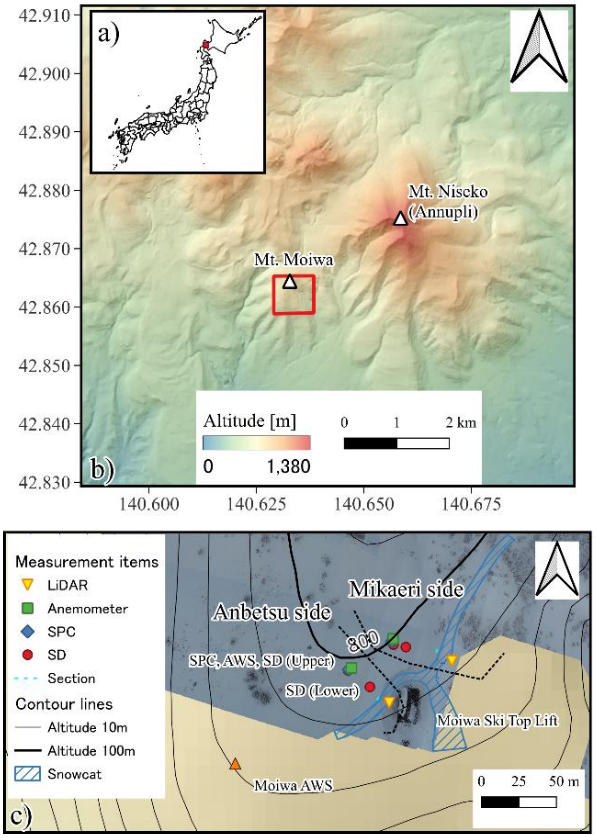

Figure 1: Geographical conditions of the study area. (a) The geographical location of this study in Japan is marked by a red square. (b) Overview of the study area. Colors indicate elevation. (c) Topography and instrument locations near the observation sites. The elevation contours represent the snow-free ground surface.

2. MATERIALS AND METHODS

2.1 Observation

To monitor snow cornice development, field observations were conducted on 6-7 February and 7-8 March 2026 near the summit lift of Niseko Moiwa Ski Resort, Hokkaido, Japan (Fig. 1). This paper focuses on the latter event. The observation site is located at an elevation of approximately 790 m. The ski resort operates an automatic weather station (referred to as the Moiwa AWS in Fig. 1(c)) that records 10-min mean wind speed, wind direction, and air temperature for operational purposes. These data were used to characterize the meteorological conditions during the observation period.

According to observations from the Automated Meteorological Data Acquisition System (AMeDAS) station at Kutchan, operated by the Japan Meteorological Agency, the cumulative hourly snowfall during the campaign period was 5 cm. The AMeDAS Kutchan station is located approximately 11 km southeast of the observation site at an elevation of 176 m. All times in this paper are given in Japan Standard Time (JST; UTC+9).

Artificial vertical snow sections were excavated at the edge of the snowpack prior to the onset of blowing snow conditions. Each section had an initial height of approximately 1.2 m and a width of more than 2 m (Fig. 2(a)). The sections exposed the temporal evolution of the snow structure on both the windward and leeward sides of the vertical face.

Cornice development was monitored on these sections. On the windward side, wind speed and direction and blowing-snow mass flux were

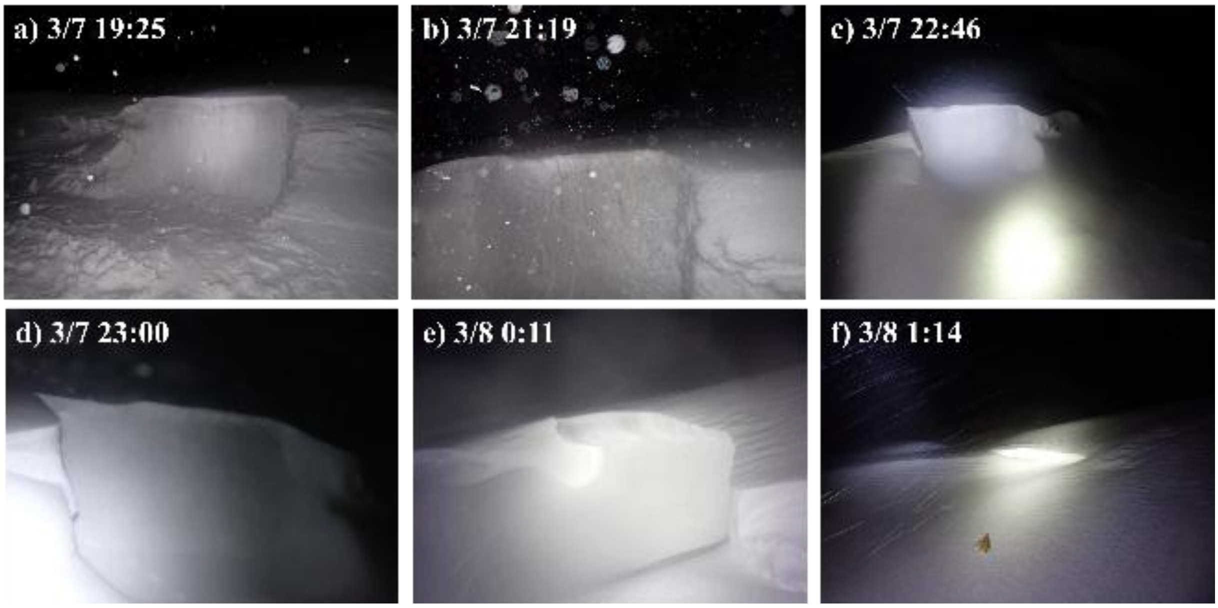

Figure 2: Photographs showing snow cornice development at the Anbetsu side, (a) 19:25, (b) 21:19, (c) 22:46, and (d) 23:00, 7 March, (e) 00:11 and (f) 01:14, 8 March.

measured at 1 Hz using ultrasonic anemometers (CALYPSO instruments, CCP-ULP) and Snow Particle Counters (SPCs; Niigata denki, SPC-95), respectively, to characterize wind conditions and blowing snow. In addition, LiDAR-based measurements were conducted using a 2D line LiDAR (TAMAYA, PSP250-90) to monitor the temporal evolution of the cornice cross section and a 1D point LiDAR sensor (self-made) to measure changes in snow surface height at 1 Hz. The locations of measurement items are shown in Fig. 1(c). In addition, UAV-mounted LiDAR surveys were conducted before and after the campaign to quantify changes in snow surface morphology. The measured variables and instruments and their sampling frequencies are listed in Table 1.

Because small changes in wind direction can strongly influence cornice formation, two observation sites were prepared for the expected northwesterly and westerly wind conditions. These sites are hereafter referred to as the Anbetsu and Mikaeri sides, respectively (Fig. 1(c)). Instrument installation was completed between 16:00 and 20:00 on 7 March.

Because of ski-lift operating restrictions, the observation team left the site at approximately 08:00 on 8 March and returned after 16:00. Consequently, manual observations were not conducted during this period. Before the team left the site, the vertical section of the Anbetsu side had already been buried by deposited snow and had developed into a gentle slope following cornice formation. Instruments capable of autonomous operation continued recording until approximately 16:00 on 8 March. The pre- and post-event UAV surveys were conducted at approximately 16:00 on 7 March and 16:00 on 8 March, respectively.

Table 1: Measurement items and their sampling frequencies.

Item	***Sampling frequency***
SPC	1 Hz
Anemometer	1 Hz
Snow depth sensor	1 Hz
2D Line LiDAR	Every 10 min or 1 min
Visual observation	At least every 60 min
UAV	Start/end of the campaign

2.2 Data Processing

The wind data were processed to obtain 10-min mean wind speed and wind direction. In addition, the wind speed gust factor, G_{wind}, was defined as the maximum 3-s mean wind speed divided by the 10-min mean wind speed within each 10-min moving window.

The 1 Hz wind speed record contained approximately 7% missing data. The 3-s mean wind speed was calculated only when all three consecutive 1-Hz measurements were available; for each 10-min moving window, the mean wind speed was calculated from the available measurements; and the gust factor was retained only when at least 90% of the original 1 Hz wind measurements were available and the longest continuous data gap did not exceed 10 s. Windows that did not satisfy these quality-control criteria were excluded from the analysis.

The blowing-snow mass flux was measured using the SPC. Similar to G_{wind}, a corresponding gust factor for the blowing-snow mass flux, G_{snow}, was calculated following Naaim-Bouvet et al. (2011).

The snow depth sensor occasionally recorded spurious distance measurements due to laser scattering when numerous drifting snow particles passed through the laser beam. These outliers were removed using a Hampel filter (Person, 1999). The snow surface displacement from the initial state was then calculated as $l(t) = d(0) - d(t)$, where $d(t)$ denotes the filtered distance at time t. Positive values of $l(t)$ indicate snow deposition, whereas negative values indicate snow erosion.

Cornice development was monitored using cross-sectional profiles acquired by a 2D line LiDAR every 10 min or every 1 min during intensive observation periods together with visual observations conducted at least once per hour. Because the 2D LiDAR was mounted with a tilt angle, the point-cloud data were rotated during post-processing so that the snowcat road became horizontal in the transformed coordinate system. The 2D LiDAR profiles also contained isolated points that were likely caused by drifting snow particles passing through the laser beam; however, these points were retained without additional filtering because they did not substantially affect interpretation of the snow-surface profiles.

3. RESULTS

3.1 10-min Wind and Temperature

The 10-min mean wind speed and wind direction are shown in Figs. 3(a) and 3(b), respectively. Except for the Moiwa AWS, the anemometers were initially installed approximately 1 m above the snow surface. The sensor height of the Moiwa AWS was higher than at the Anbetsu and Mikaeri sites.

The wind speed measured at the three locations showed similar temporal variations. At the

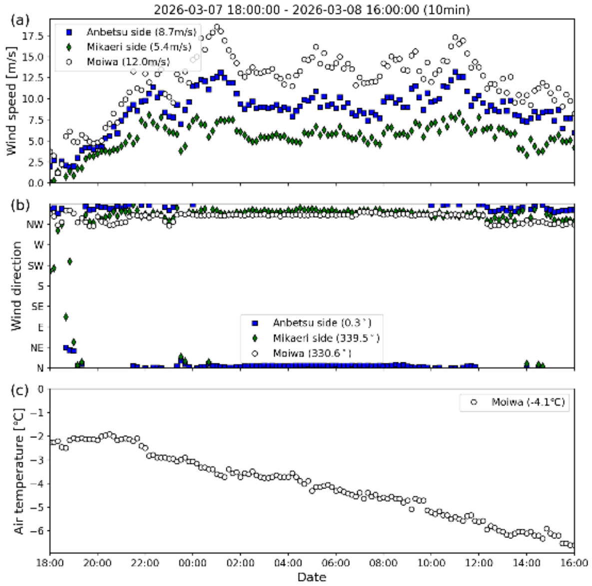

Figure 3: 10-min mean (a) wind speed, (b) wind direction, and (c) air temperature for the Anbetsu side (filled squares), the Mikaeri side (filled diamonds), and the Moiwa AWS (open circles), respectively.

Anbetsu side, the wind speed exceeded 5 m/s after 21:00 and reached a maximum of 13.1 m/s at 01:10, with predominantly northerly winds. Wind speeds above 5 m/s persisted until the end of the campaign. At the Mikaeri side, wind speed exhibited a similar temporal pattern; however, its magnitude was approximately 56% of that measured at the Anbetsu side. The prevailing wind direction at the Mikaeri side was north-northwesterly. Because both wind speed and cornice development were greater at the Anbetsu side, the following analysis focuses primarily on this location.

The 10-min mean air temperature is shown in Fig. 3(c). The air temperature was relatively high at the beginning of the campaign and gradually decreased over the observation period. It remained below 0℃ throughout the campaign.

3.2 Gust Factors for Wind Speed and Mass Flux, and Snow Height Change

Figure 4(a) shows the time series of the 10-min moving mean and standard deviation of wind speed, calculated at 1-s intervals. Despite considerable short-term fluctuations, four major local maxima in mean wind speed occurred at approximately 22:30 on 7 March and 01:00, 05:00, and 11:00 on 8 March.

Figure 4(b) shows the time series of the blowing-snow mass flux. Peaks in wind speed and blowing-snow mass flux occurred at approximately the same times; however, neither the wind-speed nor the mass-flux gust factor was consistently high during these periods (Fig. 4(c)).

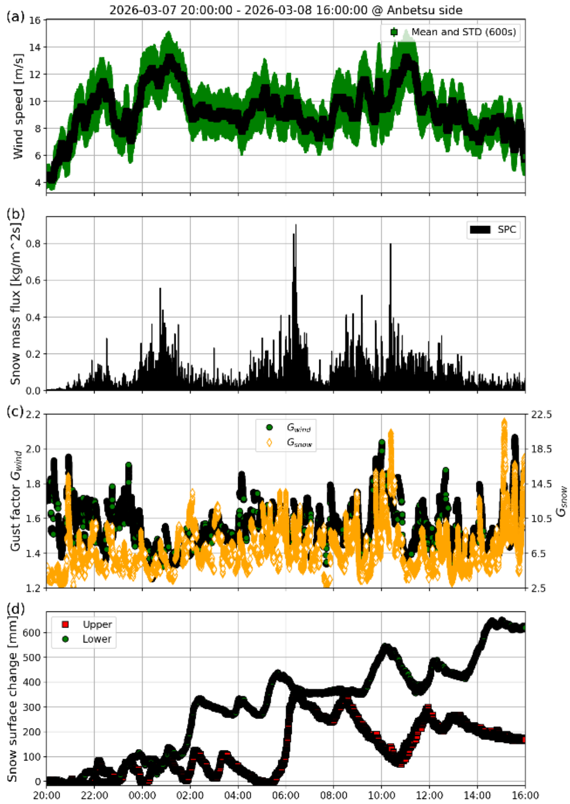

Figure 4: Time series of (a) 10-min mean wind speed and standard deviation with 10-min moving windows, (b) 1-s blowing-snow mass flux, (c) gust factors for wind G_{wind} (filled circles) and snow mass flux G_{snow} (open diamonds), and (d) snow surface height changes for Upper (filled squares) and Lower (filled circles).

Changes in snow surface height $l(t)$ at the Upper and Lower snow depth sensors are plotted in Fig. 4(d). Since the blowing-snow event was accompanied by snowfall, snow height generally increased during the campaign. At each location, sudden increases in $l(t)$ were recorded over short periods.

Note that because the Upper snow depth sensor was located close to the SPC, the changes in the local snow surface may have affected both the SPC and wind measurements by altering their effective heights above the snow surface.

3.3 Development of Snow Cornice

Figures 2 and 5 show photographs of cornice development and the vertical cross-sectional profiles obtained using the 2D line LiDAR, respectively. As shown in these figures, the snow cornice developed most rapidly around 00:00 on 8 March, with its thickness increasing by several centimeters within a 10-min period. By approximately 02:00 on 8 March, the nearly vertical cornice face had been buried by deposited snow, resulting in an almost smooth continuous slope (Fig. 5(a)).

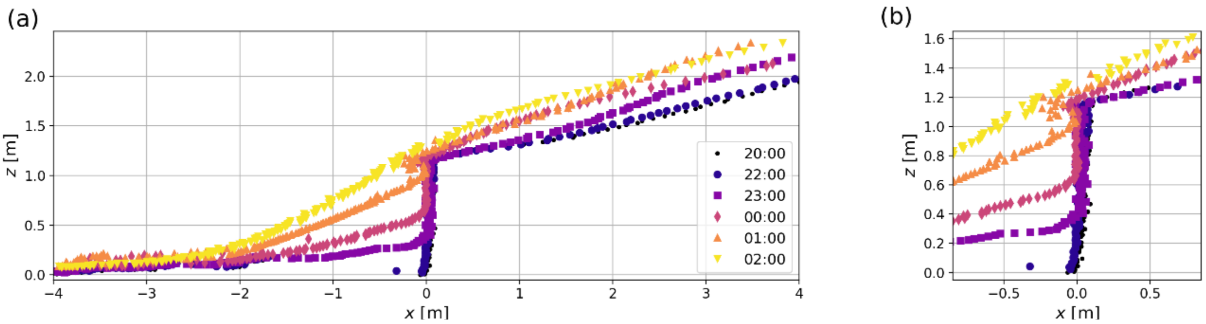

Figure 5: Vertical cross-sectional profiles of the snow cornice at (a) wide and (b) narrow scale. Colors and symbols indicate measurement times. The prevailing wind direction was from right to left.

Figure 5 suggests that the cornice development can be divided into two successive stages. On the windward side of the vertical section ($x > 0$ in Fig. 5), snow first accumulated up to approximately 2 m upstream of the cross section (corresponding to the period 20:00-23:00 on 7 March and 00:00-01:00 on 8 March). Subsequently, snow deposition occurred adjacent to the cross section (from 23:00 on 7 March to 00:00 on 8 March, and 01:00-02:00 on 8 March). The repeated alternation between these two stages gradually increased the snow height on the windward slope and produced progressive outward growth of the cornice. This pattern suggests that cornice growth was cyclic or episodic rather than spatially uniform and continuous.

On the leeward side of the cross section ($x < 0$ in Fig. 5), snow was deposited progressively, beginning immediately below the cross section. By approximately 02:00 on 8 March, the deposited snow had completely filled the vertical face and merged with the windward snowpack, forming a smooth continuous slope.

In contrast, no distinct cornice formed on the Mikaeri side during the period of valid 2D LiDAR measurements from 20:00 on 7 March to 04:30 on 8 March. During this period, snow deposition occurred immediately below the vertical section, but no overhang was observed.

3.4 Snow Redistribution

Figure 6 shows the change in snow surface elevation between the pre- and post-event UAV-mounted LiDAR surveys. Snow deposition occurred not only on the leeward side of the ridge, where the cornice developed, but also in patchy patterns on the windward side. In contrast, little evidence of substantial snow erosion was observed. Because the blowing snow event was accompanied by snowfall, snow depth generally increased across the study area.

It should be noted that a snowcat passed through part of the shown area before both the pre- and post-event UAV surveys were conducted. Consequently, the snow depth changes in these areas were affected by snowcat operations rather than by natural snow redistribution. In addition, the pre-event survey was conducted while the observation team was preparing the site, before the instruments were installed and the artificial vertical sections were excavated.

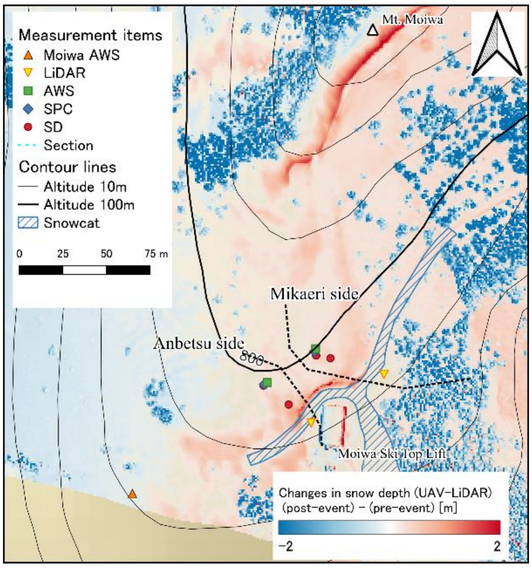

Figure 6: Difference in snow surface elevation between post- and pre-event UAV-mounted LiDAR surveys.

4. DISCUSSION

The detailed profile changes during the period of most rapid cornice growth around 00:00 are shown in Fig. 7. The high-temporal-resolution profiles indicate that outward cornice growth occurred simultaneously with an increase in the local snow depth both upwind and beneath the vertical section. These observations suggest that the cornice did not develop solely through direct attachment of snow particles to the underside of the overhang. Rather, the observations suggest that the apparent overhang developed through progressive snow accumulation around the windward slope of the vertical section.

No distinctive changes in wind speed, blowing-snow mass flux, their gust factors, or local snow-surface height were detected during the period of

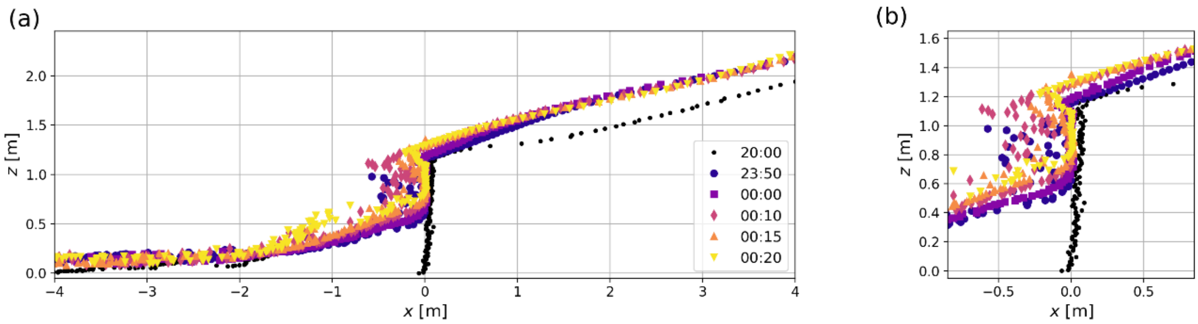

Figure 7: High-temporal-resolution vertical cross-sectional profiles of the snow cornice at (a) wide and (b) narrow scale during the period of rapid cornice growth around 00:00 on 8 March. Colors and symbols indicate measurement times. The prevailing wind direction was from right to left.

rapid cornice growth around 00:00 (Fig. 4). Therefore, the rapid growth could not be directly attributed to any single measured variable. Further investigation using computational fluid dynamics may clarify how flow separation, recirculation, and local variations in particle trajectories around the vertical section control the observed deposition pattern (Tanji, 2021; Yu et al., 2025b).

As shown in Fig. 4(d), the snow height changes around 00:00 were not large, with fluctuations of less than 10 cm. In contrast, changes exceeding 20 cm over short periods were observed after the cornice formed, e.g., 06:00 at the Upper sensor and 02:00 at the Lower sensor. These fluctuations may reflect the passage or development of wind-induced snow surface microtopography, including ripples and step-like patterns (Kochanski et al., 2019). In fact, spatiotemporal inhomogeneous surface patterns were observed by the visual observations. Such microtopographic features may affect the cornice formation directly or indirectly by influencing blowing-snow mass transport (Kosugi et al., 1992, Kochanski et al., 2019).

As shown in Figs. 2, 5 and 7, the observed cornice development involved both the outward extension of the cornice from the upper part of the cross section and the simultaneous increase in snow depth beneath it. These two processes eventually merged, resulting in the formation of a continuous snow slope. An internal cavity was observed beneath an apparently smooth snow surface during this merging process (Fig. 8). Such hidden cavities may produce mechanically weak zones within wind-deposited snow and could potentially contribute to subsequent collapse.

On the Mikaeri side, no distinct overhanging cornice developed; instead, a smooth snow slope gradually formed. The contrast between the Mikaeri and Anbetsu sides may be attributable to differences in wind speed, wind direction, blowing-snow transport, local topography, snow particle trajectories, or a combination of these factors, although the dominant cause remains unclear. Measurements (Aksamit and Pomeroy, 2016) or simulations (Yu et al., 2025b) of snow particle trajectories around the vertical sections may provide important information for identifying the dominant formation mechanism. A better understanding of the conditions that control snowdrift and cornice development would contribute to improved safety management in snow-covered mountain environments, highlighting the need for continued field observations.

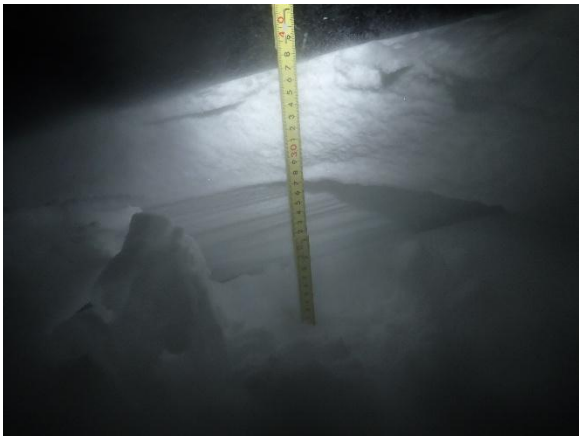

Figure 8: Internal cavity observed within a wind-deposited snowdrift on 7 February 2026.

5. CONCLUSION

This study reported snow cornice fomation around an artificial vertical snow section near the summit lift of a ski resort during 7–8 March 2026. The campaign combined measurements of wind conditions, blowing-snow mass flux, snow surface height, 2D cross-sectional profiles, UAV-LiDAR topography, and visual observations. Continuous 2D line LiDAR measurements captured the temporal evolution of cornice geometry and surrounding snowpack at intervals as short as 1 min.

The observations revealed that, on the windward side of the cross section, snow first accumulated at locations several meters upstream of the cross section and was subsequently deposited near the cross section. The observed cornice developed through repeated deposition first farther upwind and then immediately adjacent to the vertical section. On the leeward side, snow accumulated immediately beneath the cross section, and the snow surface gradually rose until it eventually merged with the overhanging cornice, forming a smooth continuous slope. No distinctive changes in the measured wind conditions, blowing-snow mass flux, or their gust factors were identified during the period of rapid cornice growth.

The observations also revealed that the cornice formation process can produce internal weak structures that may contribute to subsequent cornice collapse or avalanche release. These findings improve our understanding of short-term cornice formation and provide a basis for better assessment of cornice stability and winter mountain hazards.

ACKNOWLEDGEMENTS

The authors sincerely appreciate the support provided by Akio Shinya of the Niseko Avalanche Institute and the staff of Niseko Moiwa Ski Resort. This study was supported by JSPS KAKENHI Grant Numbers JP21H04601 (HaMaNAS PJ), JP22K03747, and JP24K17489.

REFERENCES

Aksamit, N. O. and Pomeroy, J. W. 2016. Near-surface snow particle dynamics from particle tracking velocimetry and turbulence measurements during alpine blowing snow storms, *The Cryosphere*, **10**, 3043–3062, https://doi.org/10.5194/tc-10-3043-2016.

Hancock, H., Eckerstorfer, M., Prokop, A., and Hendrikx, J. 2020. Quantifying seasonal cornice dynamics using a terrestrial laser scanner in Svalbard, Norway, *Nat. Hazards Earth Syst. Sci.*, **20**, 603–623, https://doi.org/10.5194/nhess-20-603-2020.

Kochanski, K., Anderson, R. S., and Tucker, G. E. 2019. The evolution of snow bedforms in the Colorado Front Range and the processes that shape them, *The Cryosphere*, **13**, 1267–1281, https://doi.org/10.5194/tc-13-1267-2019.

Kosugi, K., Nishimura, K. and Maeno, N. 1992. Snow ripples and their contribution to the mass transport in drifting snow. *Boundary-Layer Meteorol.* **59**, 59–66. https://doi.org/10.1007/BF00120686.

Naaim-Bouvet, F., Naaim, M., Bellot, H., Nishimura, K., 2011. Wind and drifting-snow gust factor in an Alpine context. *Ann. Glaciol.* **52**, 223–230. https://doi.org/10.3189/172756411797252112.

Pearson, R. K., 1999. Data cleaning for dynamic modeling and control. *European Control Conference (ECC)*, doi:10.23919/ECC.1999.7099714.

Tanji, S., Inatsu, M. and Okaze, T. 2021. Development of a snowdrift model with the lattice Boltzmann method. *Prog Earth Planet Sci* **8**, 57. https://doi.org/10.1186/s40645-021-00449-0.

Vogel, S., Eckerstorfer, M., and Christiansen, H. H. 2012. Cornice dynamics and meteorological control at Gruvefjellet, Central Svalbard, *The Cryosphere*, **6**, 157–171, https://doi.org/10.5194/tc-6-157-2012.

Yu, H., Guang, L., Walter, B., Huang, J., Huang, N., and Lehning, M. 2025a. Snow particle motion in process of cornice formation, The Cryosphere, 19, 5389–5402, https://doi.org/10.5194/tc-19-5389-2025.

Yu, H., Li, G., Jafari, M., Lehning, M.,Huang, J., and Huang, N., 2025b. Effect of snow cornice formation on wind fields and snow deposition: Insights from numerical simulations. *Journal of Geophysical Research: Atmospheres*, **130**, e2024JD042702. https://doi.org/10.1029/2024JD042702.

Yu, H., Li, G., Walter, B., Lehning, M., Zhang, J., and Huang, N. 2023. Wind conditions for snow cornice formation in a wind tunnel, *The Cryosphere*, **17**, 639–651, https://doi.org/10.5194/tc-17-639-2023.